J. Fluid Mech. (1970), *vol.* 42, *part* 3, *pp.* 447–464
Printed in Great Britain

On the oscillations of harbours of arbitrary shape

By LI-SAN HWANG
Tetra Tech, Incorporated, Pasadena, California, U.S.A.
AND ERNEST O. TUCK
University of Adelaide, Adelaide, Australia

(Received 21 January 1969 and in revised form 23 January 1970)

A theory is developed for calculating oscillations of harbours of constant depth and arbitrary shape. This theory is based on the solution of a singular integral equation. Numerical results have been calculated for rectangular harbours so as to check the accuracy of the method. Examples for wave amplification factor and velocity field for both rectangular and actual complex-shaped harbours are given.

1. Introduction

The occurrence of resonance in harbours is fundamentally due to the fact that waves arriving at a widening or narrowing (or at a depth increase or decrease) are partially reflected. Consider, for example, a rectangular harbour open to the sea. Waves arriving within the harbour are reflected seaward by the rear boundary; these outgoing waves, upon reaching the harbour entrance again, are partially reflected by the sudden widening, with the net result that part of the wave energy which got in does not get back out. This trapping of energy by the harbour leads to resonance if the phases of the various incident and reflected waves happen to be such that reinforcement occurs. In this case, the amplitude of oscillation may grow, within the harbour, to values far greater than those incident. At some stage of growth, however, energy dissipation and radiation equals energy trapping and the oscillation amplitude reaches its maximum. The dissipation is of three main forms: wave breaking within the harbour when the oscillation exceeds the breaking limit, frictional effects at the bottom, and wave absorption on the bounding beaches. However, radiation seaward is generally more important than all of these.

The problems of developing a practical calculation procedure applicable to these processes, already difficult, are compounded by the facts that harbours are usually of complex shape and that incident waves are never periodic. Irregularity of shape causes complicated reflexions of the waves within the harbour so that even for periodic input the agitation may appear highly irregular. The response to random sea or swell or to a dispersive wave train generated by a localized disturbance is still more difficult to analyze. Furthermore, oscillations may be induced by other mechanisms such as fluctuations in atmospheric conditions, currents moving past the entrance which generate a series of alternating

vortices, and even ship transit in and out of the harbour. It is no wonder, then, that taken in its entirety the problem of harbour resonance is intimidating.

Yet, some form of solution must be found since the harbour resonance problem is of very great practical importance in coastal engineering. This is particularly so in connexion with ship mooring problems. It is well known that harbour oscillations of only a few inches may excite large motions in ship-mooring systems causing mooring lines to break, and ships to collide with adjacent structures. To minimize such events is the goal of harbour and breakwater design, and for that purpose one must be able to determine harbour response characteristics.

Analytical studies in this area are, for the most part, quite recent. McNown (1952) determined the resonant frequency of a circular harbour with a small opening under the assumption that the entrance remains as a node of a standing wave; a similar approach was applied by Kravtchenko & McNown (1955) to the rectangular harbour. Miles & Munk (1961) considered harbours of arbitrary shape and formulated an integral equation describing the agitation within the harbour by matching conditions inside and outside the harbour at the entrance. But they imposed the restrictions of narrow openings, and slim and rectangular harbours, in order to obtain analytical expressions for the resonant conditions and maximum amplification. Ippen & Goda (1963) applied Fourier transformation methods and obtained the solution of the rectangular harbour by matching the wave amplitude and velocity approximately at the entrance. The results were compared with a series of experiments. For long harbours, the agreement between theory and experiment was good except, of course, at the resonance point where viscous dissipation is important and the experiments become difficult. Biesel & Le Méhauté (1955, 1956) and Le Méhauté (1960, 1961) presented an interesting approach in the solution of a rectangular harbour under various types of entrance conditions through the use of the theory of complex numbers. Most recently, Leendertse (1967) has developed a numerical procedure to determine the response of basins to long waves, elevation at open boundaries being prescribed.

All of the foregoing studies suffer to some degree from various deficiencies; either they are applicable only to idealized shapes or matching conditions are required at the harbour entrance. The present study requires no prescribed entrance conditions, and permits solution for completely arbitrary shape. Furthermore, the present method is highly economical for practical use since the numerical scheme involved does not require long computing time (computation time for both the results of figures 4 and 9 is less than one minute on the CDC 6600).

2. Theoretical formulation

Assuming that the fluid is inviscid, incompressible, and irrotational, there exists a velocity potential $\Phi(x, y, z; t)$ which satisfies the Laplace equation

$$\nabla^2\Phi = 0 \tag{2.1}$$

throughout the fluid contained within the boundary surfaces as shown in figure 1. If the wave is assumed to be of small amplitude, the velocity term in the Bernoulli equation may be neglected. Thus, the governing dynamic boundary condition on the free surface becomes

$$\zeta = -\frac{1}{g}\frac{\partial \Phi}{\partial t} \quad \text{at} \quad z = 0, \tag{2.2}$$

where ζ is the wave elevation and g is gravitational acceleration.

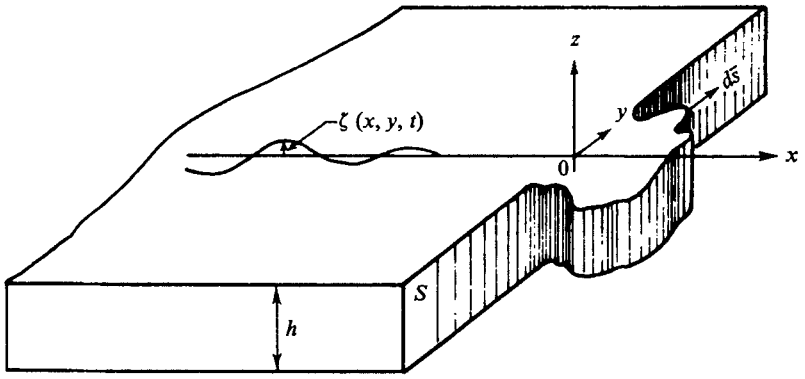

FIGURE 1. A schematic drawing of the harbour.

The linearized kinematic condition at the free surface, which follows from the fact that surface water particles stay on the surface, is expressed in the form

$$\partial \zeta / \partial t = \partial \Phi / \partial z \quad \text{at} \quad z = 0. \tag{2.3}$$

The condition on the fixed boundary surface is that the velocity normal to the surface equals zero; that is

$$\partial \Phi / \partial n = 0 \tag{2.4}$$

on the boundary S.

Since we are dealing with uniform water depth h, the condition at the bottom is simply

$$\partial \Phi / \partial z = 0 \quad \text{at} \quad z = -h. \tag{2.5}$$

Finally, the condition at infinity requires that

$$\Phi = \Phi_0 + \Phi_1, \tag{2.6}$$

$$\Phi_0 = \cos(kx \cos\beta) \exp[-i(\omega t - ky \sin\beta)], \tag{2.7}$$

and

$$\Phi_1 \text{ is an outgoing wave.} \tag{2.8}$$

The above equations complete the formulation of the problem of oscillation in a constant depth harbour of arbitrary shape.

Since the water depth is uniform, we may assume that the velocity potential is a product of functions of x and y, z, and t, such as

$$\Phi(x, y, z; t) = (1/\omega i)\, \phi(x, y)\, Z(z)\, e^{-i\omega t}, \tag{2.9}$$

where ω is the angular frequency.

Substituting the above expression into the Laplace equation, separating the functions of x and y, and z and equating them to a constant, say k^2, we have

$$\frac{\partial^2\phi}{\partial x^2}+\frac{\partial^2\phi}{\partial y^2}+k^2\phi = 0 \tag{2.10}$$

and

$$\frac{\partial^2 Z}{\partial z^2}-k^2 Z = 0. \tag{2.11}$$

The solution of (2.11) together with the bottom boundary condition

$$\partial Z/\partial z = 0 \quad \text{at} \quad z = -h \tag{2.12}$$

and the kinematic surface boundary condition

$$\zeta = -\frac{1}{g}\frac{\partial\Phi}{\partial t}\bigg|_{z=0} = A\phi(x,y)\,e^{-i\omega t} \tag{2.13}$$

can be found in some text-books (e.g. Stoker 1963), and is simply

$$Z(z) = -Ag\cosh k(z+h)/\cosh kh, \tag{2.14}$$

where A is the amplitude of a standing wave at infinity. The constant, k, is a wave-number, and is related to the angular frequency ω and the water depth h through the kinematic boundary condition at the free surface. This relationship can be simply obtained by substituting (2.9), (2.13) and (2.14) into (2.3). One finds

$$\omega^2 = gk\tanh kh. \tag{2.15}$$

The problem now is to obtain the solution of (2.10) with the boundary condition

$$\partial\phi/\partial n = 0 \quad \text{on the solid boundary } S, \tag{2.16}$$

which is obtained from the substitution of (2.9) into (2.6), and with the prescribed condition at infinity. The condition at infinity can be determined as if the harbour were absent. This is due to the fact that the influence of radiated waves from the harbour tends to zero at infinity. Thus, for a straight-crested standing wave at infinity with the crest at an angle β to the shoreline, we have

$$\phi_0 = \cos(kx\cos\beta)\exp[-iky\sin\beta] \quad (0<\beta<\pi), \tag{2.17}$$

which corresponds to the wave form

$$\zeta = A\cos(kx\cos\beta)\exp[-i(\omega t-ky\sin\beta)] \tag{2.18}$$

at infinity. If the wave front propagates directly toward the shore, β is equal to zero, so that

$$\phi_0 = \cos kx. \tag{2.19}$$

3. Derivation of the integral equation

For a standing wave of unit amplitude at infinity, the solution of Weber's equation (2.10), together with the boundary conditions, (2.16) and (2.17), can be found through the introduction of a source function $Q(\xi,\eta)$ along the boundary S, where ξ and η refer to co-ordinates on the boundary.

Thus, the value of $\phi(x,y)$ at any point (x,y), is equal to the sum of two parts; one is the influence from infinity $\phi_0(x,y)$ and the other is the contribution of the source distribution, that is, the scattered wave caused by the presence of the boundary. The latter will be given by

$$\int_S dS\, Q(\xi,\eta)\, G(x,y;\xi,\eta), \tag{3.1}$$

where $G(x,y;\xi,\eta)$ is the Green's function and $Q(\xi,\eta)$ is the unknown source distribution, which can be determined from the boundary conditions.

The Green's function has to be chosen so that it is the solution of Weber's equation, (2.10), satisfies the radiation condition at infinity, and has a singularity at the source point. Thus we choose the Green's function to be a Hankel function of the first kind rather than of the second kind to guarantee that the disturbance, due to the harbour, at infinity takes the form of an outgoing wave rather than an incoming wave.

$$G(x,y;\xi,\eta) = -\tfrac{1}{4}iH_0^{(1)}(kR), \tag{3.2}$$

where

$$R = [(x-\xi)^2+(y-\eta)^2]^{\frac{1}{2}}, \tag{3.3}$$

so that the value of $\phi(x,y)$ at any point (x,y) is

$$\phi(x,y) = \phi_0(x,y) + \int_S dS\, Q(\xi,\eta)\, G(x,y;\xi,\eta). \tag{3.4}$$

The problem now is to determine the strength of the source distribution $Q(\xi,\eta)$. This can be accomplished by applying the boundary condition (2.16), which gives

$$\lim_{x,y\to\xi',\eta'} \left[\frac{\partial\phi_0(x,y)}{\partial n} + \frac{\partial}{\partial n}\int_S dS\, Q(\xi,\eta)\, G(x,y;\xi,\eta)\right] = 0. \tag{3.5}$$

Since the limit is singular inside the integral, it has to be treated with care. We evaluate the integral in (3.5) by use of contour integration. The path of the integral is along the boundary except around the point (ξ',η') where the contour is deformed into a small circle with a radius ϵ. Since the contribution around a large semicircle is zero, the integral in (3.5) may be evaluated as follows:

$$\begin{aligned}\lim_{x,y\to\xi',\eta'} \frac{\partial}{\partial n}\int_S dS\, Q(\xi,\eta)\, G(x,y;\xi,\eta) \\ = \text{⨍}_S dS\, Q(\xi,\eta)\, G_n(\xi',\eta';\xi,\eta) + \lim_{x,y\to\xi',\eta'}\int_\epsilon dS\, Q(\xi,\eta)\, G_n(x,y;\xi,\eta),\end{aligned} \tag{3.6}$$

where the sign ⨍_S refers to a principal value in the sense of Cauchy. Since the Hankel function can be approximated by

$$-\tfrac{1}{4}iH_0^{(1)}(kR) \to \frac{1}{2\pi}\ln(kR) \quad (R\to 0) \tag{3.7}$$

the second integral of the right-hand side of (3.6) may be integrated analytically. We have

$$\lim_{x,y\to\xi',\eta'} \frac{\partial}{\partial n}\int_\epsilon dS\, Q(\xi,\eta)\, G(x,y;\xi,\eta) = \lim_{R\to 0}\frac{1}{2\pi}Q(\xi',\eta')\int_{-\pi}^{\pi}\frac{\partial}{\partial R}\ln kR\, R\, d\theta = \tfrac{1}{2}Q(\xi',\eta'). \tag{3.8}$$

Thus the integral equation becomes

$$\tfrac{1}{2}Q(\xi',\eta')+\int\!\!\!\!\!\!-_S dS\,Q(\xi,\eta)\,G_n(kR) = -\frac{\partial}{\partial n}\phi_0(\xi',\eta'), \tag{3.9}$$

where

$$G_n(kR) = -\tfrac{1}{4}i\,\partial(H_0^{(1)}(kR))/\partial n. \tag{3.10}$$

The above equation cannot be solved analytically. A numerical method for evaluating the source distribution $Q(\xi,\eta)$ is derived in the following section.

4. Numerical solution

Let us divide the boundary S into many segments with length ΔS_j along the boundary, where $j = 1, 2, 3, \ldots, N$. The lengths of these segments need not be uniform; however, they must be small enough so that within each segment, the source strength $Q(\xi,\eta)$ does not vary too much. Furthermore, let the midpoint of ΔS_i be (ξ_i, η_i) and evaluate the integral at this midpoint of each segment. Within each segment the source strength does not vary much, so that we take $Q(\xi,\eta)$ to be constant and equal to Q_j within ΔS_j. Then (3.9) becomes

$$\tfrac{1}{2}Q_i+\sum_{j=1}^{N} Q_j\left[\int\!\!\!\!\!\!-_{\Delta S_j} dS\,G_n(\xi_i,\eta_i;\xi,\eta)\right] = -\frac{\partial\phi_0(\xi_i,\eta_i)}{\partial n}; \tag{4·1}$$

for simplicity, we may write the above equation in the following form

$$\sum_{j=1}^{N} B_{ij}Q_j = b_i, \tag{4.2}$$

where

$$\left.\begin{aligned} B_{ij} &= \tfrac{1}{2}\delta_{ij}+\int\!\!\!\!\!\!-_{\Delta S_j} dS\,G_n(\xi_i,\eta_i;\xi,\eta),\\ b_i &= -\frac{\partial\phi_0(\xi_i,\eta_i)}{\partial n}\end{aligned}\right\} \tag{4.3}$$

and δ_{ij} is the Kronecker delta.

Equation (4.2) is an algebraic equation which can be solved easily provided the constants B_{ij} are known.

To evaluate B_{ij}, let us split $G(kR) = -\frac{1}{4}iH_0^{(1)}$ into two parts; one singular part and the regular part:

$$G(kR) = (1/2\pi)\log R + M(kR). \tag{4.4}$$

Substituting (4.4) into (4.2), we have

$$B_{ij} = \tfrac{1}{2}\delta_{ij}+\frac{1}{2\pi}\int\!\!\!\!\!\!-_{\Delta S_j} dS\frac{\partial}{\partial n}\log R+\int\!\!\!\!\!\!-_{\Delta S_j}\frac{\partial M}{\partial n}\,dS. \tag{4.5}$$

The first integral on the right-hand side of the equation can be calculated analytically and is

$$\frac{1}{2\pi}\int\!\!\!\!\!\!-_{\Delta S_j} dS\frac{\partial}{\partial n}\log R = \frac{\Delta\theta_{ij}}{2\pi}, \tag{4.6}$$

where $\Delta\theta_{ij}$ is the angle subtended at (ξ_i,η_i) by the segment of S between (X_j, Y_j) and (X_{j+1}, Y_{j+1}).

Now we fix an index i [that is, choose a point (ξ_i, η_i)] and then run over the whole set of $j = 1, 2, 3, \ldots, N$ and evaluate the angle $\Delta\theta_{ij}$ as follows:

For $i \neq j$
$$\Delta\theta_{ij} = \tan^{-1}\frac{Y_{j+1}-\eta_i}{X_{j+1}-\xi_i} - \tan^{-1}\frac{Y_j-\eta_i}{X_j-\xi_i}. \tag{4.7}$$

For $i = j$
$$\Delta\theta_{ij} = 0. \tag{4.8}$$

The last integral in (4.5) is not singular, thus the bar on the integral can be left out. It can be approximated directly to be

$$\int_{\Delta S_j} dS\, \partial M/\partial n = \Delta S_j\, \partial M/\partial n \tag{4.9}$$

and $\Delta S_j\, \partial M/\partial n$ can be evaluated as follows:

$$\begin{aligned}\Delta S_j M_n &= \Delta Y_j M_X - \Delta X_j M_Y \\ &= \Delta Y_j \frac{\partial M}{\partial R}\frac{X_j-\xi_i}{R} - \Delta X_j \frac{\partial M}{\partial R}\frac{Y_j-\eta_i}{R},\end{aligned} \tag{4.10}$$

where
$$\Delta X_j = X_{j+1}-X_j, \quad \Delta Y_j = Y_{j+1}-Y_j. \tag{4.11}$$

The value of b_i in (4.2) can be obtained in a similar way, i.e.

$$\begin{aligned}-b_i &= \frac{\partial \phi_0(X_i Y_i)}{\partial n} \\ &= \frac{\partial \phi_0}{\partial x}\frac{\Delta Y}{[(\Delta X)^2+(\Delta Y)^2]^{\frac{1}{2}}} + \frac{\partial \phi_0}{\partial y}\frac{\Delta X}{[(\Delta X)^2+(\Delta Y)^2]^{\frac{1}{2}}}.\end{aligned} \tag{4.12}$$

Once the source strength Q has been calculated, the value of $\phi(x, y)$ can be evaluated as follows:

$$\begin{aligned}\phi(x,y) &= \phi_0(x,y) + \int_S dS\, Q(\xi,\eta)\, G(kR) \\ &= \phi_0(x,y) + \int_S dS\, Q(\xi,\eta)\left[\frac{1}{2\pi}\log R + M(kR)\right] \\ &= \phi_0(x,y) + \sum_j Q_j \Delta S_j M_j + \sum_j Q_j A_j,\end{aligned} \tag{4.13}$$

where
$$\begin{aligned}A_j &= \frac{1}{2\pi}\int_{\Delta S_j} \log R\, dS \\ &= \mathrm{Re}\left\{\frac{1}{2\pi}\int_{\Delta S_j} \log z\, dz\, .\, e^{i\alpha}\right\} \\ &= \mathrm{Re}\left\{\frac{1}{2\pi} e^{-i\alpha}[z_2 \log z_2 - z_2 - z_1 \log z_1 + z_1]\right\}.\end{aligned}$$

The symbols z_1, z_2 and α are as indicated in figure 2, and are related to the original system as follows (z_1 and z_2 are complex numbers):

$$\left.\begin{aligned} e^{-i\alpha} &= \frac{X_{j+1}-X_j-i(Y_{j+1}-Y_j)}{\Delta S_j}, \\ \Delta S_j &= [(X_{j+1}-X_j)^2+(Y_{j+1}-Y_j)^2]^{\frac{1}{2}}, \\ z_2 &= (X_{j+1}-\xi_i)+i(Y_{j+1}-\eta_i) \\ \text{and} \quad z_1 &= (X_j-\xi_i)+i(Y_j-\eta_i).\end{aligned}\right\} \tag{4.14}$$

Once the value of $\phi(x, y)$ is known, the velocity potential can be calculated from (2.9).

$$\Phi(x, y, z; t) = -\frac{Ag}{\omega i}\phi(x, y)\frac{\cosh k(z+h)}{\cosh kh}e^{-i\omega t}, \tag{4.15}$$

where $\phi(x, y)$ is the value obtained from (4.13).

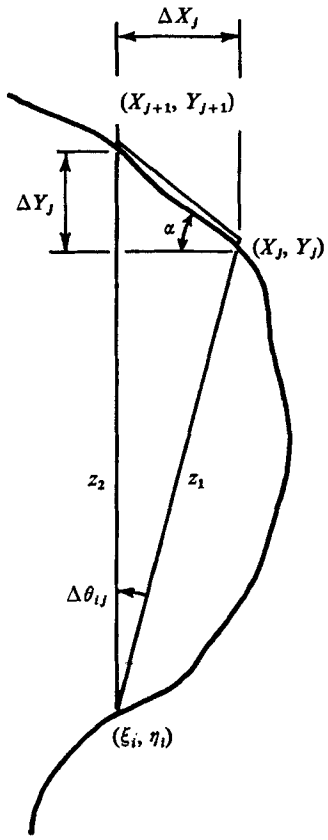

FIGURE 2. Co-ordinates used to evaluate the integral $\frac{1}{2\pi}\int_{\Delta S_j} dS \log R$.

The velocity components at any location (x, y, z) can be calculated as

$$u = -\frac{\partial \Phi_r}{\partial x} = -\frac{Ag}{\omega}\left[\frac{\partial \phi_i}{\partial x}\cos\omega t - \frac{\partial \phi_r}{\partial x}\sin\omega t\right]\frac{\cosh k(z+h)}{\cosh kh}, \tag{4.16}$$

$$v = -\frac{\partial \Phi_r}{\partial y} = -\frac{Ag}{\omega}\left[\frac{\partial \phi_i}{\partial y}\cos\omega t - \frac{\partial \phi_r}{\partial y}\sin\omega t\right]\frac{\cosh k(z+h)}{\cosh kh}, \tag{4.17}$$

where the subscripts i and r refer to the imaginary and real parts of the complex values, respectively.

The amplification factor at any point (x, y) is equal to the ratio of maximum wave height obtained at point (x, y) to the wave height at infinity. The maximum

wave amplitude at infinity is A. However, the maximum wave amplitude at point (x, y) is

$$\zeta_{\max} = \left| -\frac{1}{g}\frac{\partial \Phi}{\partial t}\bigg|_{z=0} \right| = A\,|\phi(x, y)|.$$

Thus the amplification factor at any point (x, y) is simply

$$R = |\phi(x, y)|. \tag{4.18}$$

The actual choice of number and distribution of segments around the harbour is necessarily largely intuitive. The results presented in this paper were computed with about 60 segments, distributed fairly evenly around the harbour and extending to about two wavelengths along the straight outside edges. Essentially the same results (to an accuracy of better than one per cent inside the harbour) were obtained using 40 segments, either by truncating closer to the harbour entrance (say at one wavelength distance) or by reducing the overall density of segments. Generally speaking, a density of eight segments per wavelength was found to be satisfactory, with more points where the shoreline changes rapidly or at points of special interest.

5. Results and discussion

To check the accuracy of the numerical results obtained by the present theory, a rectangular harbour of dimension $12{\cdot}25 \times 2{\cdot}38$ inches was chosen first for numerical calculation. This particular harbour geometry has been studied both analytically and experimentally by Ippen & Goda (1963); therefore, a comparison of their results with the results obtained by the present theory can be made. Furthermore, this is a relatively long harbour, so that Ippen & Goda's approximations should be acceptable, and our results should agree with theirs.

Figure 3 shows the frequency response of the rectangular harbour. The experimental results are indicated by the small circles, while the theoretical results obtained by Ippen & Goda are the solid curve. The dotted line was calculated by the present theory. All results were calculated and measured at location A as shown on the figure. Both theoretical curves are in agreement with the experimental data except around the fundamental mode.

The scattering of the experimental amplification factors, around the fundamental mode of resonance, has been indicated by Ippen & Goda to be due to inefficiency of the wave energy dissipators for incident waves of very low steepness. For low wave steepness, the transmission coefficient of wave filters increases, and their effectiveness for dissipation becomes small. Thus, the incident waves generated by the wave paddle were interfered with by the waves radiated from the wall.

The experimental results are lower than theory close to the fundamental periods. This is probably due to energy dissipation generated by eddies around the entrance and friction along the side wall and bottom, which has not been considered in either theory.

As shown in figure 3, in the immediate neighbourhood of the fundamental period, the results obtained by the present theory are slightly larger than those

reported by Ippen & Goda. These differences are probably due to the result of approximation used by Ippen & Goda.

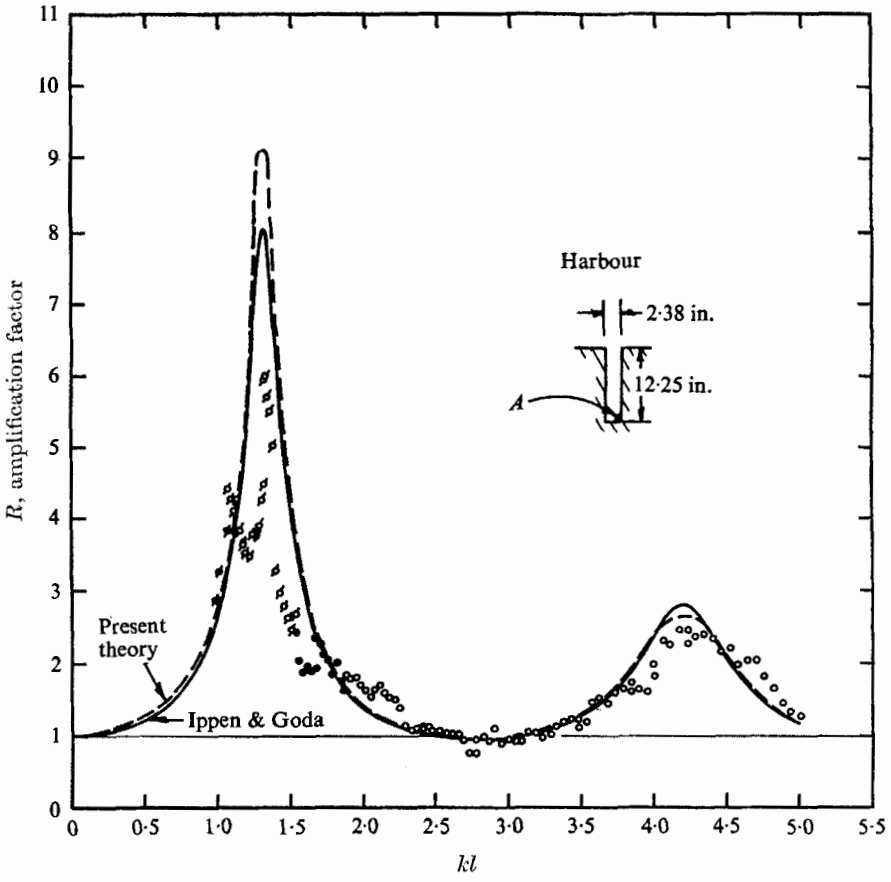

FIGURE 3. A comparison of theoretical and experimental results for frequency response of a fully open harbour.

Typical amplification fields of wave height for the rectangular harbour were calculated by use of (4.18). The results of these calculations are plotted in figures 4, 5 and 6. The units indicated on the figures represent the scale of the wave height relative to the incoming wave height. The results plotted in figures 4 and 5 are for kl equal to 1·3 and 4. They are located near the fundamental and the first harmonic, respectively. Thus the maximum wave height inside the harbour is larger than the wave height outside the harbour. Furthermore, it is interesting to point out that the waves outside the harbour entrance do not decrease uniformly as the distance from the harbour increases. Instead, they exhibit a modulation phenomenon which results from the superposition of the radiated waves and the incident waves. The results plotted in figures 4 and 6 have the same wave-number, but a different incident angle. It is clear that the amplification factor in figure 6 is considerably less than that in figure 4. This is

expected because the effective wave-number decreases when the incident wave is at an angle, and the effective frequency of excitation is further away from the fundamental period of oscillation.

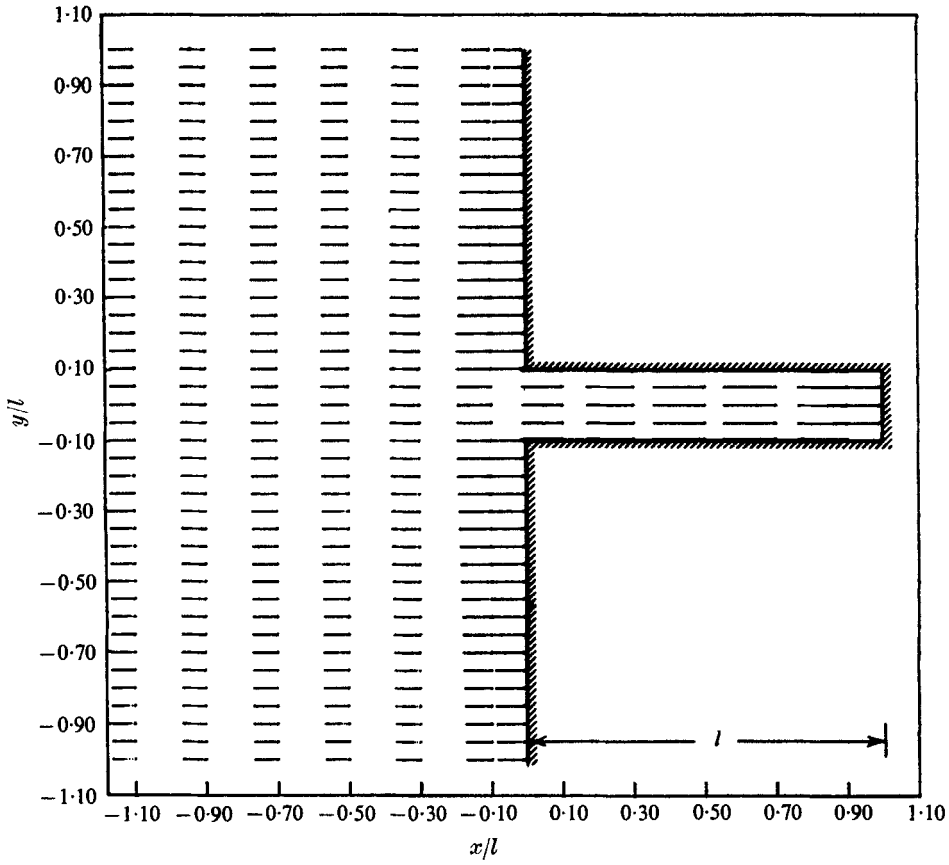

FIGURE 4. Amplification factor field of the wave height at $kl = 1{\cdot}3$, $\beta = 0°$. ——— 15 units.

Figures 7 and 8 show the amplification factor of the wave height for a bay with a complex shape. In the case where the wave-number is small (long waves), the water level inside the entire harbour oscillates almost uniformly; thus the amplification factor is more or less uniform inside the harbour as shown in figure 7.

In contrast, in figure 8, the incident wavelength L is relatively short in comparison to harbour length l ($L \approx 1{\cdot}5l$). The oscillations inside the harbour become rather complicated. Each basin inside the harbour may develop its own mode of oscillation, and at the same time may also affect the oscillation of a neighbouring basin. Such mutual interaction may be referred to as a 'coupling oscillation'. Thus, in determining oscillations of a harbour with multiple basins, one cannot treat each basin separately without considering these interaction phenomena. As can be seen in figure 7, there is hardly any nodal line at the entrance of the bay, while in figure 8, one may identify a nodal line near the entrance. The

presence and location of such a nodal line is not only a function of harbour geometry but also depends on the frequency of the incoming wave. A solution with an imposed condition at the entrance is, therefore, not the solution of the actual problem. Such a condition has often been assumed (McNown 1952;

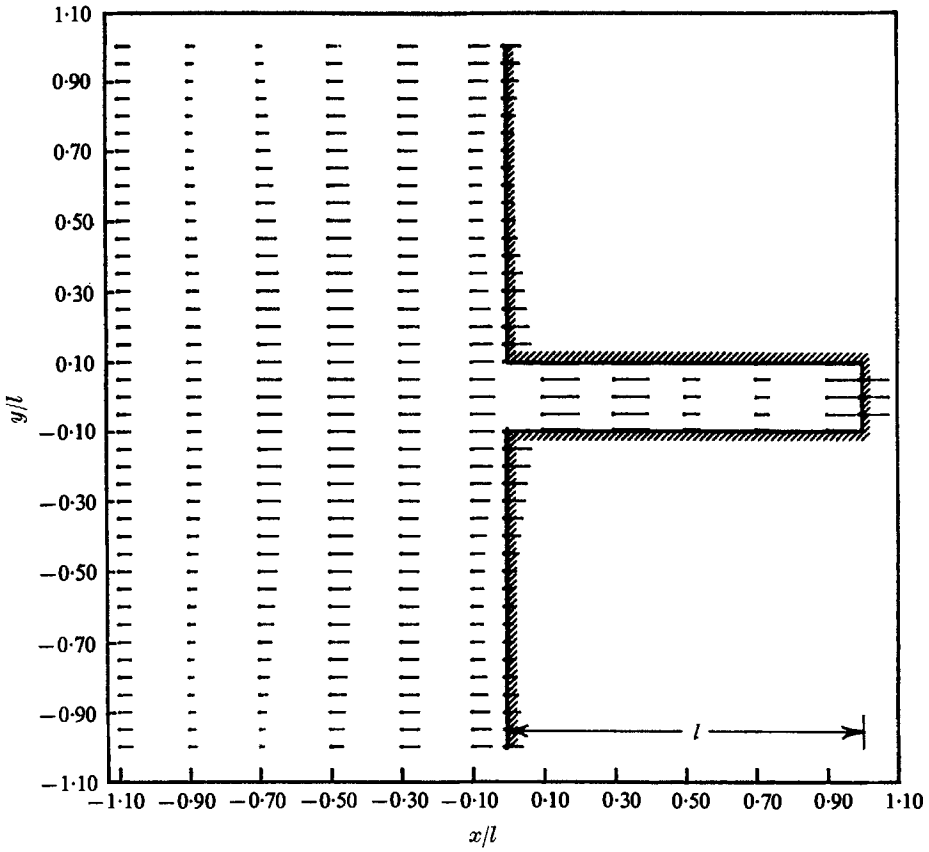

FIGURE 5. Amplification factor field of the wave height at $kl = 4$, $\beta = 0°$. ——— 6 units.

Wilson, Hendrickson & Kilmer 1965; Leendertse 1967; Loomis 1966). In particular, the use of the assumption of a nodal line at the entrance may introduce a large degree of inaccuracy, and may sometimes lead to wrong conclusions. With a complicated open harbour, it is, in any case, quite arbitrary what we might call the 'entrance'.

The velocity at any point can be calculated from (4·16) and (4.17). At the free surface, the velocity can be obtained simply by letting $z = 0$ so that

$$u = -\frac{\partial \Phi_r}{\partial x} = -\frac{Ag}{\omega}\left[\frac{\partial \phi_i}{\partial x}\cos\omega t - \frac{\partial \phi_r}{\partial x}\sin\omega t\right], \tag{5.1}$$

$$v = -\frac{\partial \Phi_r}{\partial y} = -\frac{Ag}{\omega}\left[\frac{\partial \phi_i}{\partial y}\cos\omega t - \frac{\partial \phi_r}{\partial y}\sin\omega t\right]; \tag{5.2}$$

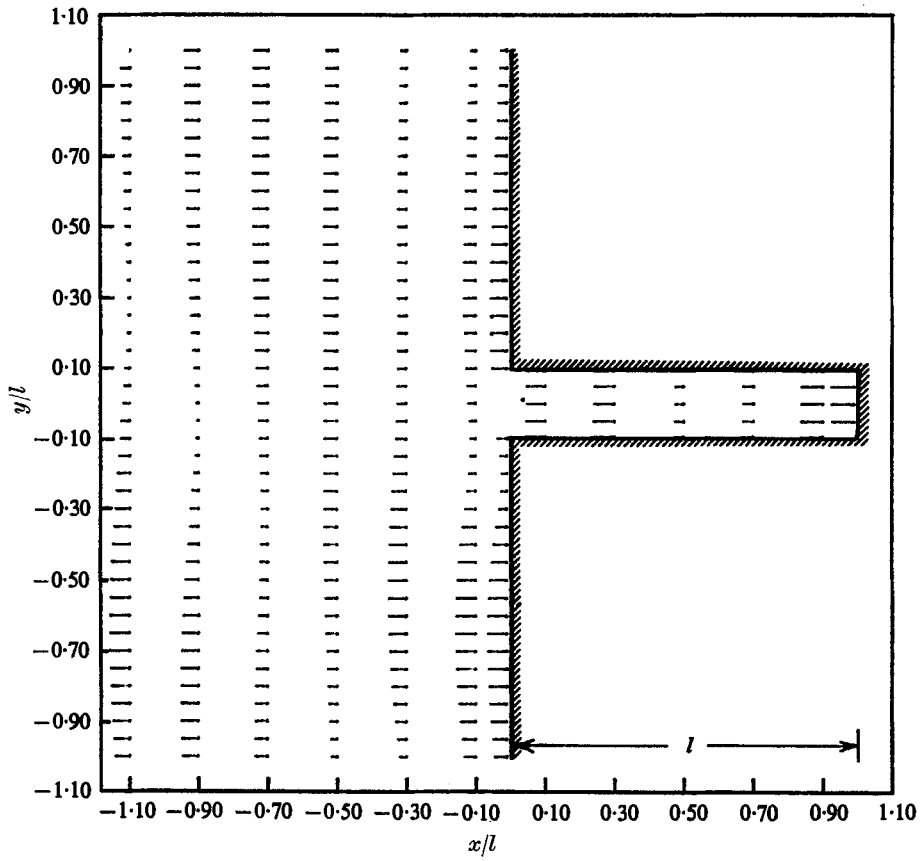

FIGURE 6. Amplification factor field of the wave height at $kl = 4$, $\beta = 45°$. ——— 6 units.

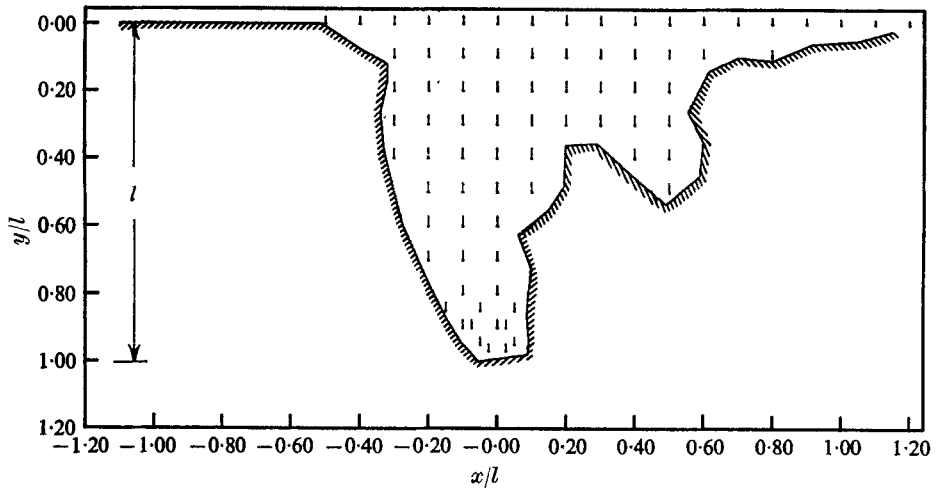

FIGURE 7. Amplification factor field of the wave height in an arbitrarily shaped bay at $kl = 1{\cdot}3$, $\beta = 0°$. ——— 12 units.

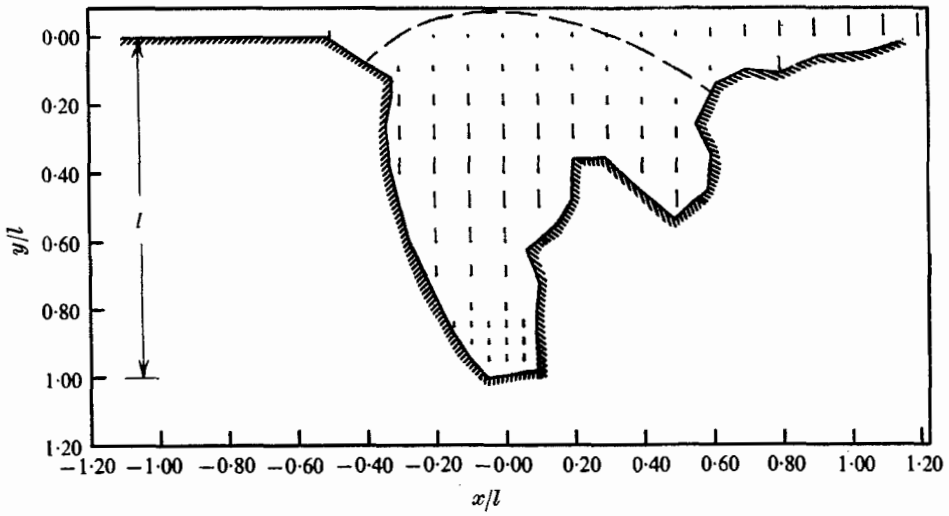

FIGURE 8. Amplification factor field of the wave height in an arbitrarily shaped bay at $kl = 4$, $\beta = 0°$. ——— 5 units.

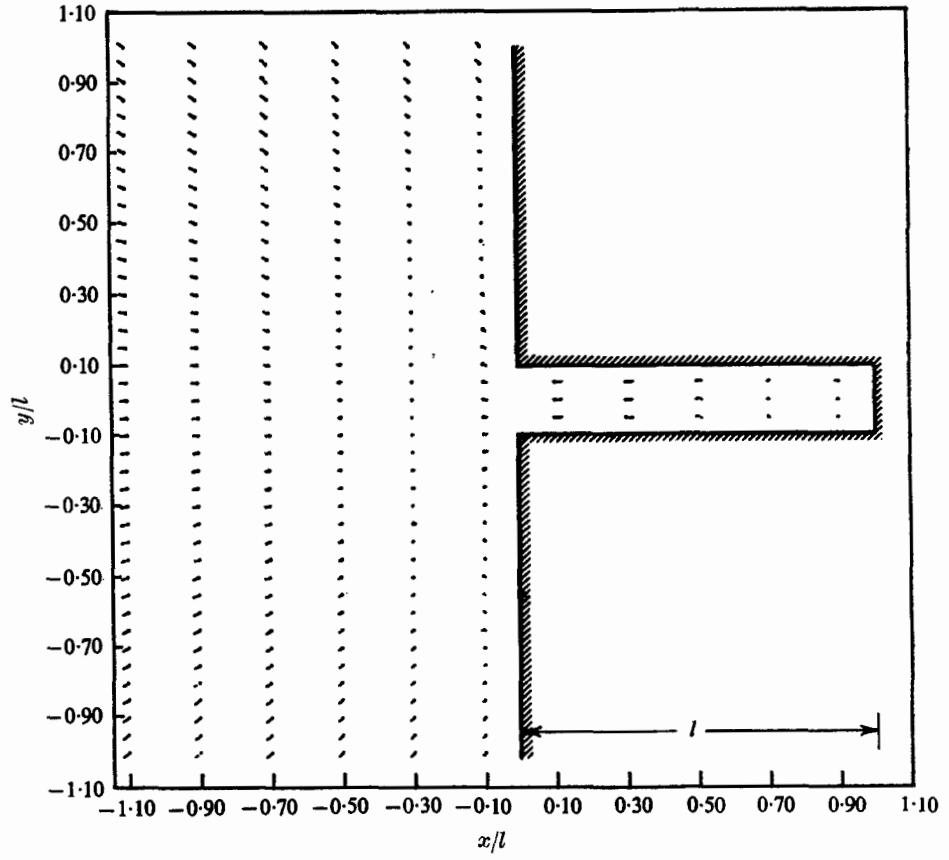

FIGURE 9. Velocity field in a rectangular harbour at $kl = 1{\cdot}3$, $\beta = 0°$. ——— 50 units.

from the above equations, it is clear that at a given point the magnitude and the direction of the velocity varies from time to time and the period of such variation equals the period of the incoming waves.

Figures 9 and 10 show the velocity field of the rectangular harbour corresponding to the phase $\omega t = \frac{1}{2}\pi$ with $kl = 1{\cdot}3$ and 4. The small line segments on

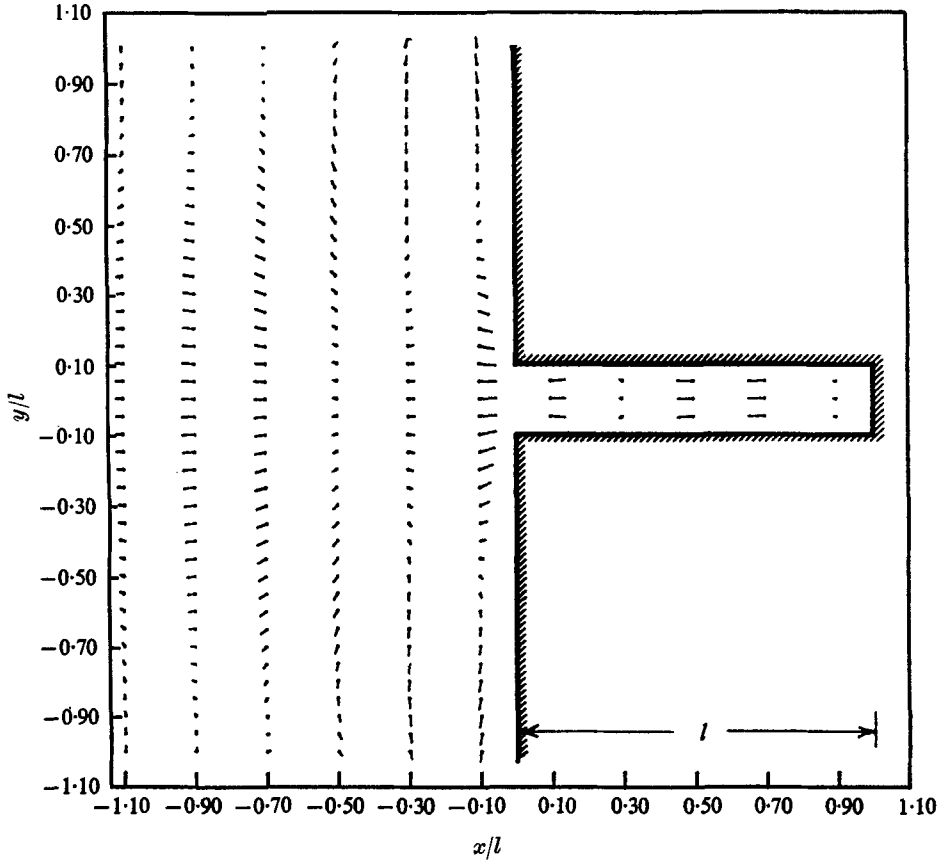

FIGURE 10. Velocity field in a rectangular harbour at $kl = 4$, $\beta = 0°$.
——— 16 units.

the figures indicate the magnitude and the direction of the velocity. The small black dots at the ends of the line segments indicate the locations where the velocity was calculated. The line pointing away from the black dot indicates the direction of the velocity. Figure 9 indicates that the velocity vectors around the harbour, at that instant, point toward the harbour entrance. This inflow of water in all directions around the entrance results in an increase of wave elevation inside the harbour. The magnification of the wave amplitude inside the harbour is associated with the proper match of the inflow of water with the outflow from the reflexions on the harbour boundary. If the characteristics of the harbour are such that the outflow and the inflow of water are properly matched with the incident wave, resonance is achieved. The wave-number or period for which the proper match can be achieved is a characteristic of the harbour.

Figure 11 shows the velocity field for $kl = 4$, but the incident wave is at an angle $\beta = 45$ degrees with the shoreline. The velocity outside the harbour is not symmetric with respect to the centreline. However, inside the harbour, the velocity pattern is still relatively uniform due to the relative narrowness of the harbour.

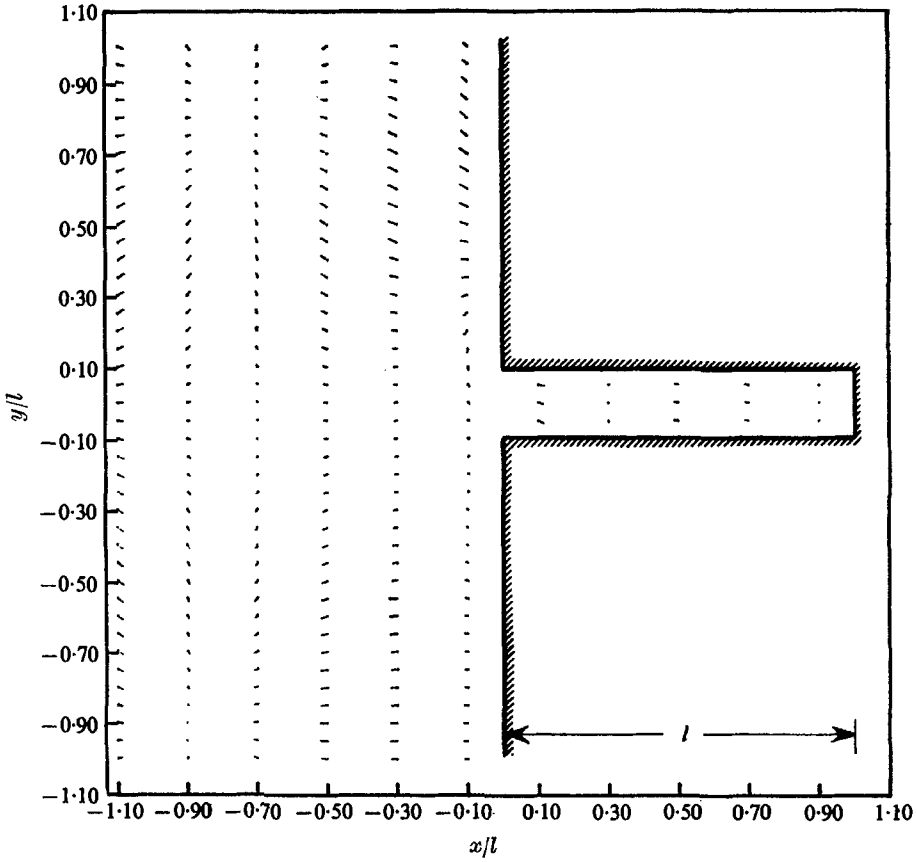

FIGURE 11. Velocity field in a rectangular harbour at $kl = 4$, $\beta = 45°$. ——— 30 units.

Figure 12 (plate 1) shows two reproduced photos of path-line patterns taken by Ippen & Goda. These two photos were taken at periods $T = 0{\cdot}6$ and $0{\cdot}5$ sec, as indicated in the figures. The velocity patterns shown on figures 9–11 exhibit some resemblance to the path-line patterns indicated in figure 12, although no quantitative agreement is to be expected since the harbour dimensions are different.

Figures 13 and 14 show the velocity field of an arbitrarily shaped bay. It is interesting to see that the velocity inside the harbour is not uniform. The existence of such complicated motions results from the phase lag of the reflected wave from the complex boundary. Such a complicated motion is more pronounced when the incident wave period becomes small, as can be seen from a comparison of figures 13 and 14.

This work was sponsored by the Atomic Energy Commission under contract AT(26-1)-289(M 002).

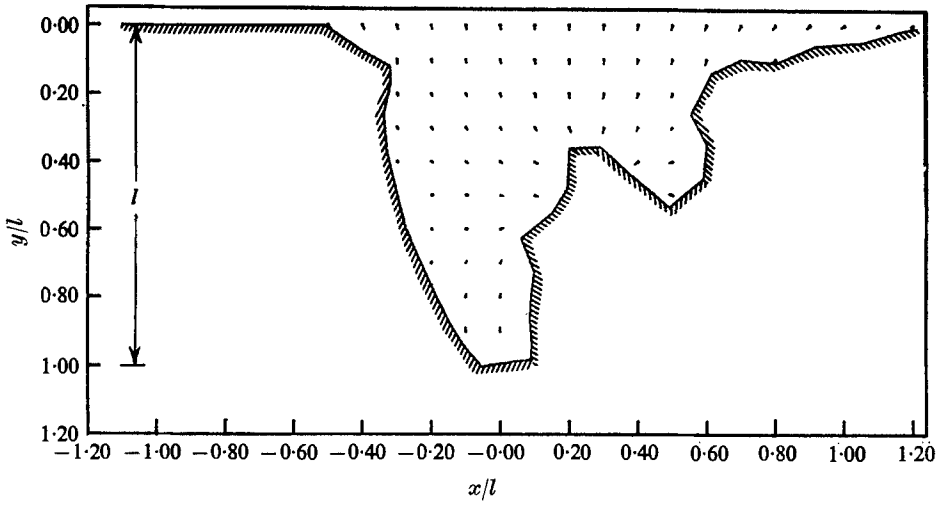

FIGURE 13. Velocity field in an arbitrarily shaped bay at $kl = 1{\cdot}3$, $\beta = 0°$. ——— 20 units.

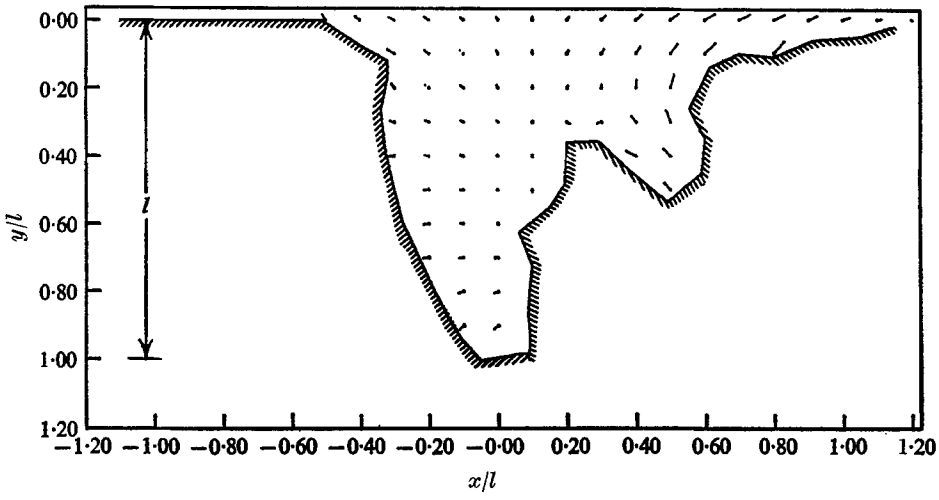

FIGURE 14. Velocity field in an arbitrarily shaped bay at $kl = 4$, $\beta = 0°$. ——— 15 units.

REFERENCES

BIESEL, F. & LE MÉHAUTÉ, B. 1955 Etude theorique de la reflexion de la houle sur certains obstacles. *La Houille Blanche*, pp. 130–140.

BIESEL, F. & LE MÉHAUTÉ, B. 1956 Mouvements de resonance a deux dimensions dans une enceinte sous l'action d'ondes incidentes. *La Houille Blanche*, pp. 348–374.

IPPEN, A. T. & GODA, Y. 1963 Wave induced oscillations in harbours: The solution for a rectangular harbour connected to the open sea. *Hydro Lab., Mass. Inst. of Tech.*

KRAVTCHENKO, J. & MCNOWN, J. S. 1955 Seiche in rectangular ports. *Quart. Appl. Math.* **13**, 19–26.

LEENDERTSE, JAN J. 1967 Aspects of a computational model for long period water-wave propagation. *Rand Co. Report* no. RM-5294-PR.

LE MÉHAUTÉ, B. 1960 Periodical gravity wave on a discontinuity. *J. Hydraulics Div. ASCE*, pp. 11–41.

LE MÉHAUTÉ, B. 1961 Theory of wave agitation in a harbour. *J. Hydraulics Div. ASCE*, no. 2765.

LOOMIS, H. 1966 Some numerical hydrodynamics for Hilo harbour, Hawaii. *Institute of Geophysics, University of Hawaii.*

MCNOWN, J. S. 1952 Waves and Seiche in idealized ports. *Gravity Waves Symposium*, National Bureau of Standards, Circular 521.

MILES, J. & MUNK, W. 1961 Harbour paradox. *Journal of Waterways and Harbours Division, ASCE*, no. 2888.

STOKER, J. J. 1963 *Water Waves.* New York: Interscience.

WILSON, B. W., HENDRICKSON, J. A. & KILMER, R. E. 1965 Feasibility study for surge-action model of Monterey harbour, California. *U.S. Army Engineers, WES, Corps of Engineers.*

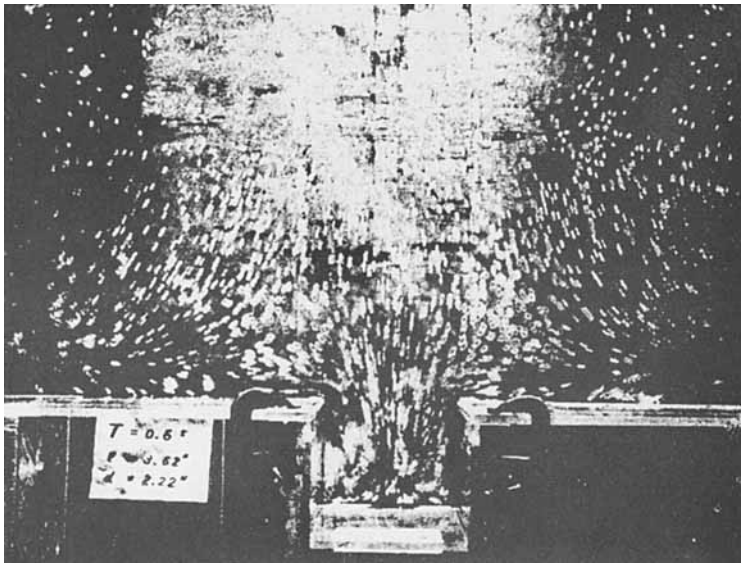

Resonance (T = 0·6 sec).

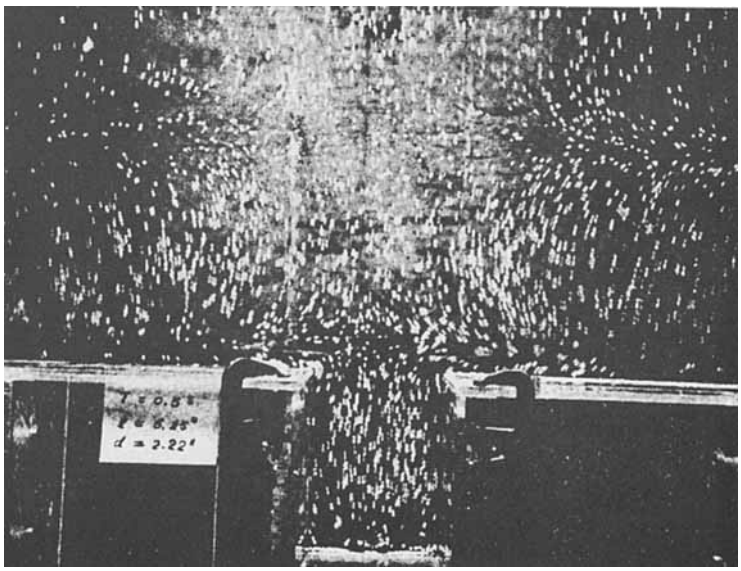

Anti-Resonance (T = 0·5 sec).

FIGURE 12. Path-line pattern (reproduced from Ippen & Goda 1963).